Electronic Supplementary Material (ESI) for Inorganic Chemistry Frontiers.

Supporting information for the paper:

High proton conductivity modulated by active protons in 1D ultra-stable metal-organic coordination polymers：a new insight into coordination interaction/ability of metal ion

Xiaoqiang Liang, [*a] Sen Wang, [a] Siqing Zhang, [a] Chenyang Lin, [a] Fengxia Xie, [a] Renzhong Li, [*a] Feng Zhang,[*c] Chen Wen, [b] Lei Feng [b] and Chengan Wan [b]

[a] *College of Environmental and Chemical Engineering, Xi'an Polytechnic University, Xi'an 710048, PR China*

[b] *Beijing Spacecrafts, Beijing 100094, PR China*

[c] *Key Laboratory of Photochemical Biomaterials and Energy Storage Materials, Heilongjiang Province and College of Chemistry and Chemical Engineering, Harbin Normal University, Harbin 150025, PR China*

Table of Contents

Section	Content	Page
I	Crystallographic data	S3−S5
II	Characterization: PXRD patterns	S6
III	Characterization: IR spectra	S7
IV	Characterization: XPS survey spectra	S8
V	Characterization: SEM images	S9
VI	Stability: TGA curves	S10
VII	Stability: Nitrogen sorption measurements	S11-12
VIII	Stability: IR Spectra	S13
IX	Stability: PXRD pattern and IR spectrum of Mn-pzdc-H_3O^+ after being treated with boiling water	S14
X	Water adsorption–desorption isotherms	S15
XI	Electrochemical measurements: impedance spectra	S16−S21
XII	PXRD patterns after impedance measurements.	S22
XIII	Comparison of chemical stability	S23
XIV	Comparison of proton conductivity	S24−S25
XV	References for Supporting Information	S26−S27

I. Crystallographic data

Table S1 Crystallographic data and details of refinements for previously reported **Zn-pzdc-H_3O^+**, **Mn-pzdc-H_3O^+** and **Cu-Hpzdc-H_2O**.[1-3]

Compounds	Zn-pzdc-H_3O^+	Mn-pzdc-H_3O^+	Cu-Hpzdc-H_2O
Empirical formula	$C_{12}H_{10}N_4O_{10}Zn$	$C_{12}H_{10}N_4O_{10}Mn$	$C_{12}H_{10}N_4O_{10}Cu$
*M*r	453.62	425.17	433.77
Crystal system	Monoclinic	Monoclinic	Monoclinic
Space group	*C2/c*	*C2/c*	$P2_1/n$
a (Å)	14.478(3)	14.484 (2)	6.6163(14)
b (Å)	8.439(2)	8.480 (1)	14.174(2)
c (Å)	12.861(3)	13.087 (1)	8.5821(14)
α (°)	90	90	90
β (°)	114.66(3)	114.753 (7)	97.62(2)
γ (°)	90	90	90
V (Å^3)	1428.05	1459.71	797.7(2)
Z	4	4	2
D_c (g cm^{-3})	2.026	1.93	1.806
μ(mm^{-1})	1.79	0.901	1.436
F(000)	880	n/a	438
Collected reflections	1986	3855	3511
Unique reflections	1628	2039	1407
Parameters	143	144	137
T (K)	293	293	294
Final R_1 [a], wR_2[b]	0.0334, 0.1045	0.0332, 0.0242	0.0410, 0.0830
	[$F_o > 4\sigma(F_o)$]	[$F_o > 3\sigma(F_o)$]	[$I > 2\sigma(I)$]
GOF	1.104	n/a	1.071
	[$F_o > 4\sigma(F_o)$]		[$I > 2\sigma(I)$]
Largest peak and hole (e ·Å^{-3})	0.84, −0.38	0.4, −0.4	n/a, n/a

Table S2 Selected bond lengths (Å) and angles (°) for previously reported **Zn-pzdc-H_3O^+**, **Mn-pzdc-H_3O^+** and **Cu-Hpzdc-H_2O**. [1-3]

Zn-pzdc-H_3O^+			
Zn(1)−O(4)	2.071(2)	Zn(1)−O(4a)	2.071(2)
Zn(1)–N(2)	2.184(2)	Zn(1)−N(2a)	2.184(2)
Zn(1)−O(1b)	2.092(2)	Zn(1)−O(1c)	2.092(2)
O(4)−Zn(1)−O(1b)	105.94(6)	O(4)−Zn(1)−O(1c)	88.11(6)
O(4)−Zn(1)−N(2)	77.27(6)	O(4)−Zn(1)−O(4a)	161.68(7)
N(2)−Zn(1)−N(2b)	106.68(7)	N(2) −Zn(1)−O(1b)	159.09(7)
N(2)−Zn(1)−O(4a)	91.73(6)	N(2)−Zn(1)−O(1c)	88.40(7)
O(1b)−Zn(1)−O(1c)	81.26(7)		
Mn-pzdc-H_3O^+			
Mn(1)−O(3)	2.137(1)	Mn(1)−O(1)	2.153(1)
Mn(1)–N(2)	2.307(2)	Mn(1)−O(3a)	2.137(1)
Mn(1)−O(1a)	2.153(1)	Mn(1)−N(2a)	2.307(2)
O(3)−Mn(1)−O(3a)	82.62(7)	O(3)−Mn(1)−O(1)	106.92(4)
O(3)−Mn(1)−O(1)	90.45(4)	O(3)−Mn(1)−N(2)	158.44(4)
N(2)−Mn(1)−N(2a)	106.83(9)	O(3a)− Mn(1)−N(2a)	88.01(5)
O(1b)−Mn(1)−N(2a)	73.71(5)	O(1)−Mn(1)−N(2a)	92.48(5)
O(1)−Mn(1)−O(1a)	157.05(5)		
Cu-Hpzdc-H_2O			
Cu(1)−O(1)	1.947(3)	Cu(1)−N(1)	1.997(3)
Cu(1)−O(4b)	2.401(3)	Cu(1)−O(1a)	1.947(3)
Cu(1)−N(1a)	1.997(3)	Cu(1)−O(4c)	2.401(3)
O(1)−Cu(1)−O(1a)	180.0	O(1)−Cu(1)−O(4b)	94.24(10)
O(1)−Cu(1)−N(1a)	96.80(11)	O(1)−Cu(1)−O(4c)	85.77(10)
N(1)−Cu(1)−O(4b)	91.41(10)	O(1a)−Cu(1)−N(1a)	83.20(11)
N(1a)−Co(1)−O(4c)	88.59(10)	O(4c)−Co(1)−O(4b)	180.00(91)

Symmetry codes : a) 1−*x*, *y*, 1/2−*z*; b) *x*, 2−*y*, −1/2+*z*; c) 1−*x*, 2−*y*, −*z* for **Zn-pzdc-H_3O^+**; a) −*x*, *y*, 1/2−*z* for **Mn-pzdc-H_3O^+**; a) 2−*x*, 1−*y*, 1−*z*; b) 1−*x*, 1−*y*, 1−*z*; c) −*x*, 1−*y*, 1−*z* for **Cu-Hpzdc-H_2O**.

Table S3 Hydrogen−bonding geometry parameters (Å, °) for **Zn-pzdc-H_3O^+**, **Mn-pzdc-H_3O^+** and **Cu-Hpzdc-H_2O**. [1-3]

D−H···A	d(D−H)	d(H···A)	d(D···A)	∠(DHA)
		Zn-pzdc-H_3O^+		
O(1W)−H(1WX)···O(2)	1.03(4)	1.48(4)	2.501(3)	177(4)
O(1W)−H(1WY)···O(3d)	0.86(8)	1.81(7)	2.496(3)	136(7)
O(1W)−H(1WZ)···N(1e)	0.88(4)	1.87(4)	2.745(3)	175(4)
		Mn-pzdc-H_3O^+		
O(1W)−H(1WX)···O(4b)	1.04(3)	1.49(3)	2.518(2)	170(2)
O(1W)−H(1WY)···O(2c)	1.04(3)	1.45(3)	2.483(2)	175(3)
O(1W)−H(1WZ)···N(1d)	0.90(3)	1.86(3)	2.747(2)	175(4)
		Cu-Hpzdc-H_2O		
O(3d)−H(3d)···O(1W)	1.09(8)	1.44(8)	2.510(5)	169(7)
O(1W)−H(1WX)···O(2d)	0.68(5)	2.00(5)	2.680(5)	173(5)
O(1W)−H(1WY)···N(2e)	0.82(6)	2.03(6)	2.844(5)	175(6)

Symmetry codes: d) x −1/2, −y+3/2, z+1/2; e) x−1/2, y−1/2, z+1 for **Zn-pzdc-H_3O^+**; b) −x, y, 3/2−z; c) −x, −y,1−z; d) x, −y, 1/2+z for **Mn-pzdc-H_3O^+**; d) −1+x, y, z; e) 1−x, 1−y, −z for **Cu-Hpzdc-H_2O**.

II. Characterization: PXRD patterns

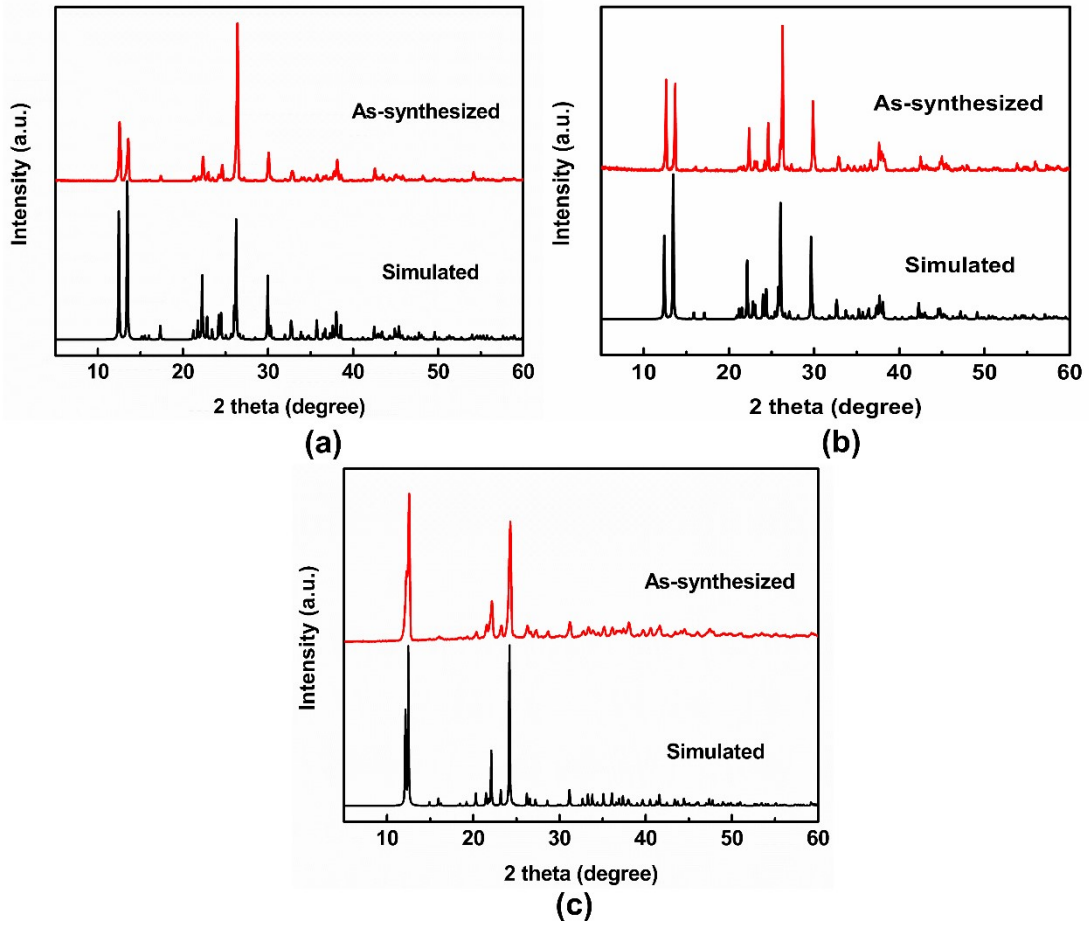

Fig. S1 (a) The PXRD patterns for **Zn-pzdc-H_3O^+** of a simulation based on single-crystal analysis and as-synthesized bulk crystals. (b) The PXRD patterns for **Mn-Hpzdc-H_3O^+** of a simulation based on single-crystal analysis and as-synthesized bulk crystals. (c) The PXRD patterns for **Cu-Hpzdc-H_2O** of a simulation based on single-crystal analysis and as-synthesized bulk crystals.

III. Characterization: IR Spectra

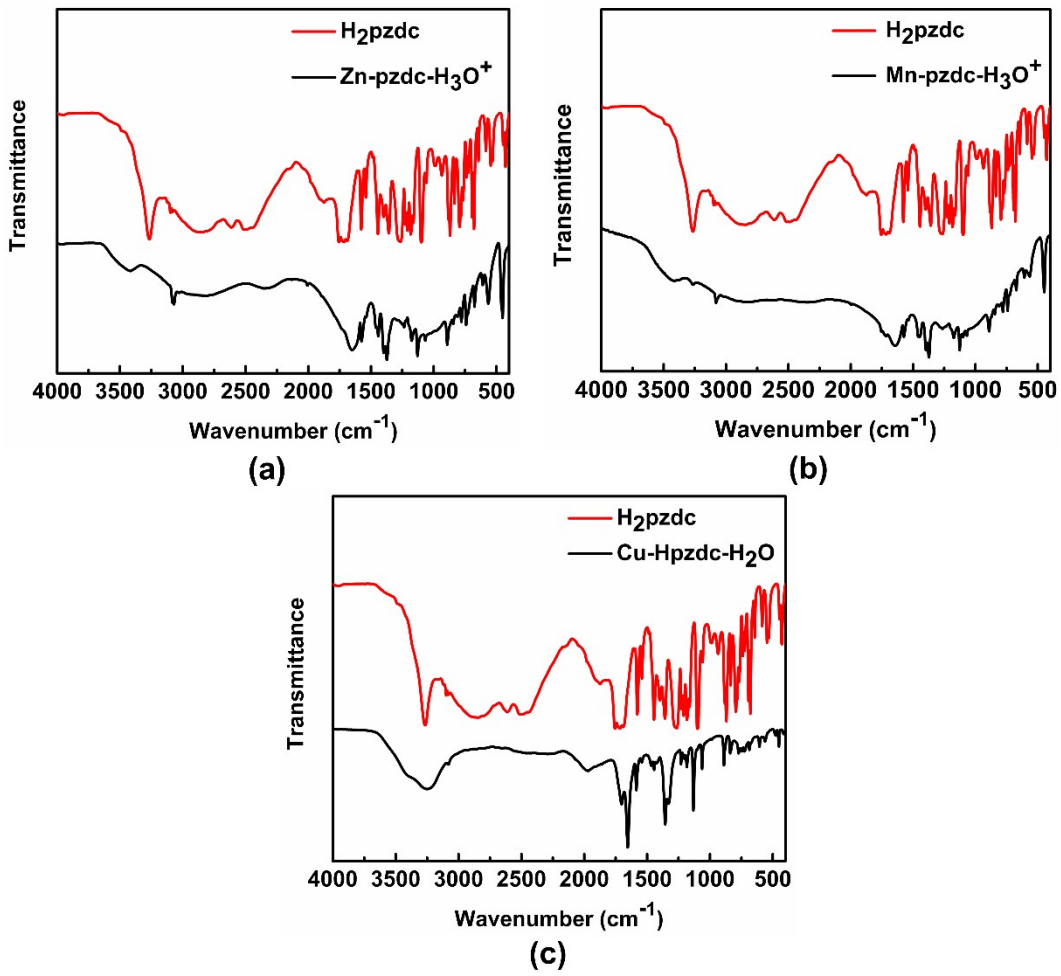

Fig. S2 (a) IR spectra of **H_2pzdc** together with **Zn-pzdc-H_3O^+** (a), **Mn-pzdc-H_3O^+** (b) and **Cu-Hpzdc-H_2O** (c) in the solid state at room temperature (performed on a Bruker IFS-66V/S FT-IR spectrometer).

IV. Characterization: XPS survey spectra

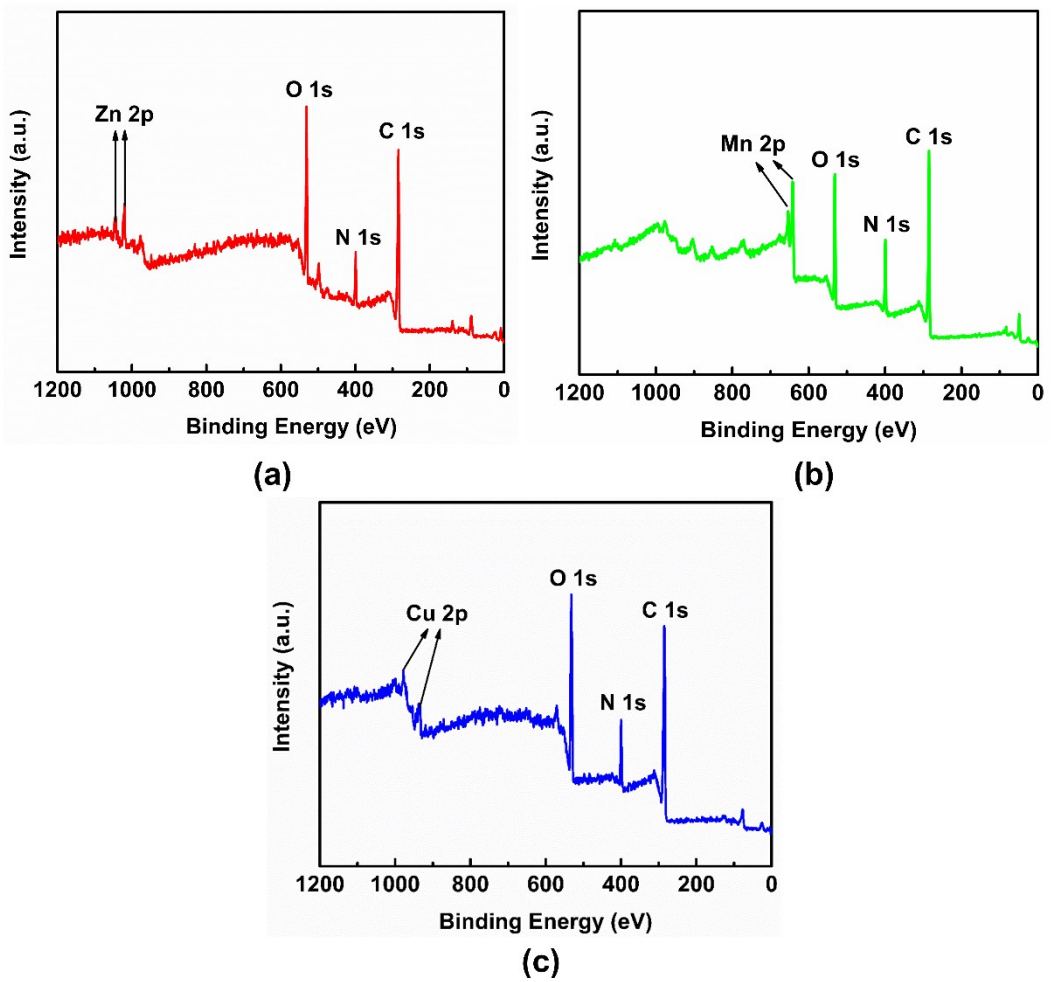

Fig. S3 XPS survey spectra of **Zn-pzdc-H_3O^+** (a), **Mn-pzdc-H_3O^+** (b) and **Cu-Hpzdc-H_2O** (c).

V. Characterization: SEM images

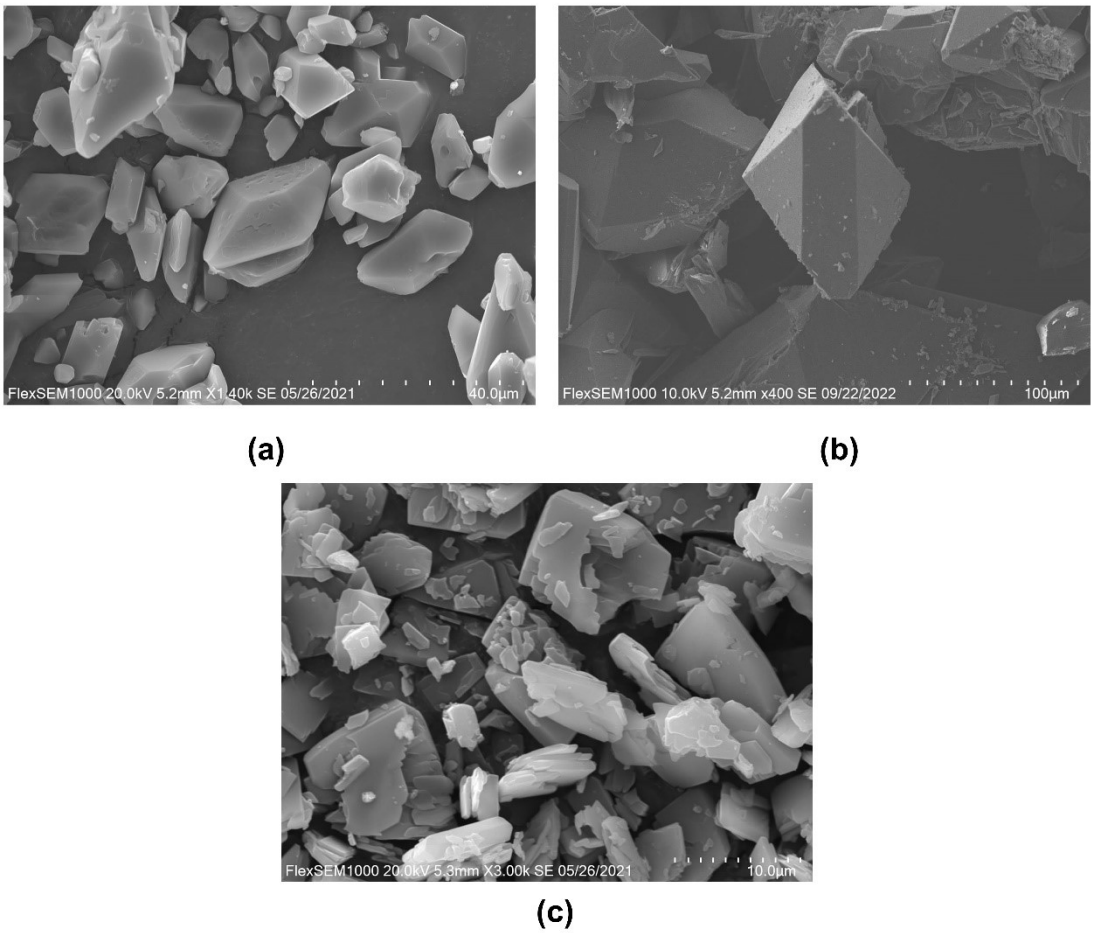

Fig. S4 SEM images of **Zn-pzdc-H_3O^+** (a), **Mn-pzdc-H_3O^+** (b) and **Cu-Hpzdc-H_2O** (c).

The SEM images reveal that Zn-pzdc-H_3O^+ and Mn-pzdc-H_3O^+ are unique polyhedral morphology with about 2–24 μm and 35-80 μm in sizes, respectively, and Cu-Hpzdc-H_2O has a uniformly sheet-like structure with size of around 0.8–11.2 μm (Fig. S4).

VI. Stability: TGA curves

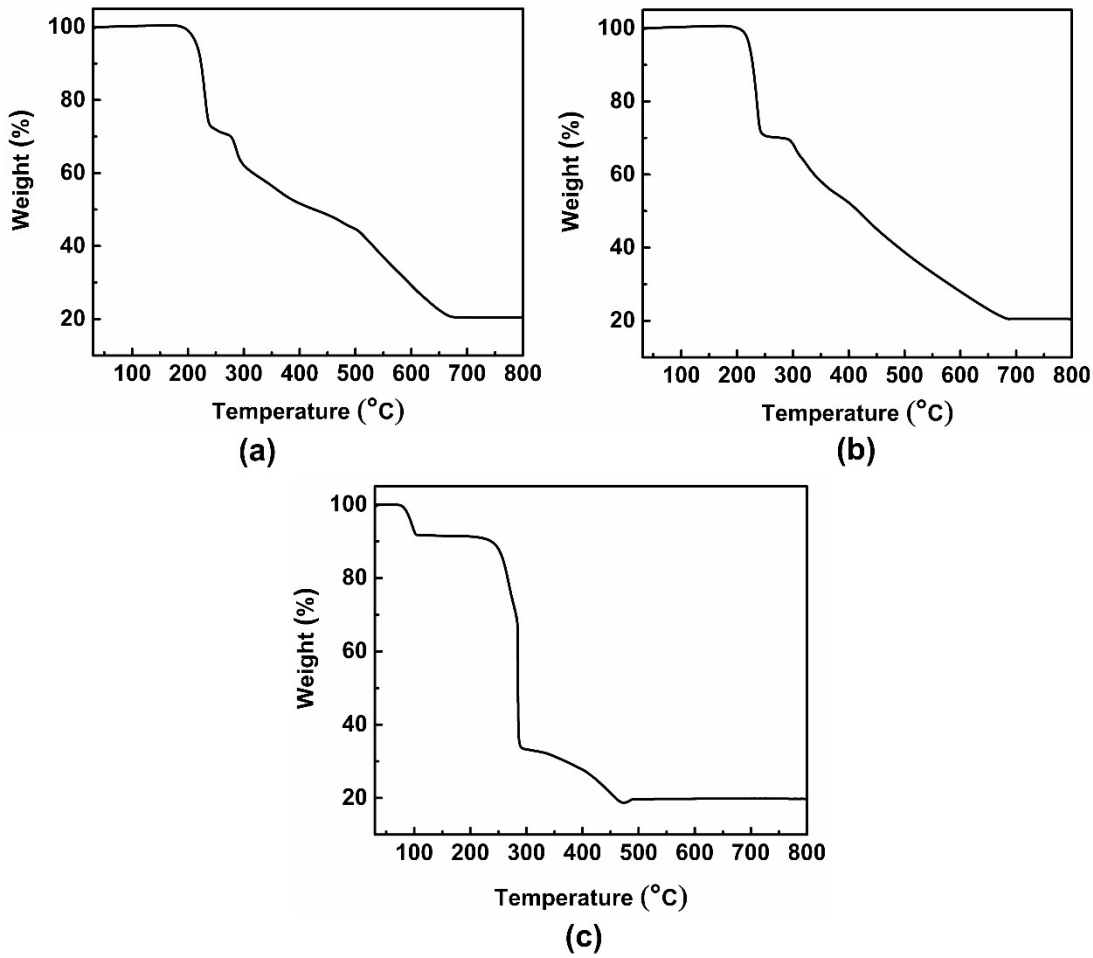

Fig. S5 Thermogravimetric curves for **Zn-pzdc-H_3O^+** (a), **Mn-pzdc-H_3O^+** (b) and **Cu-Hpzdc-H_2O** (c).

VII. Stability: Nitrogen sorption measurements

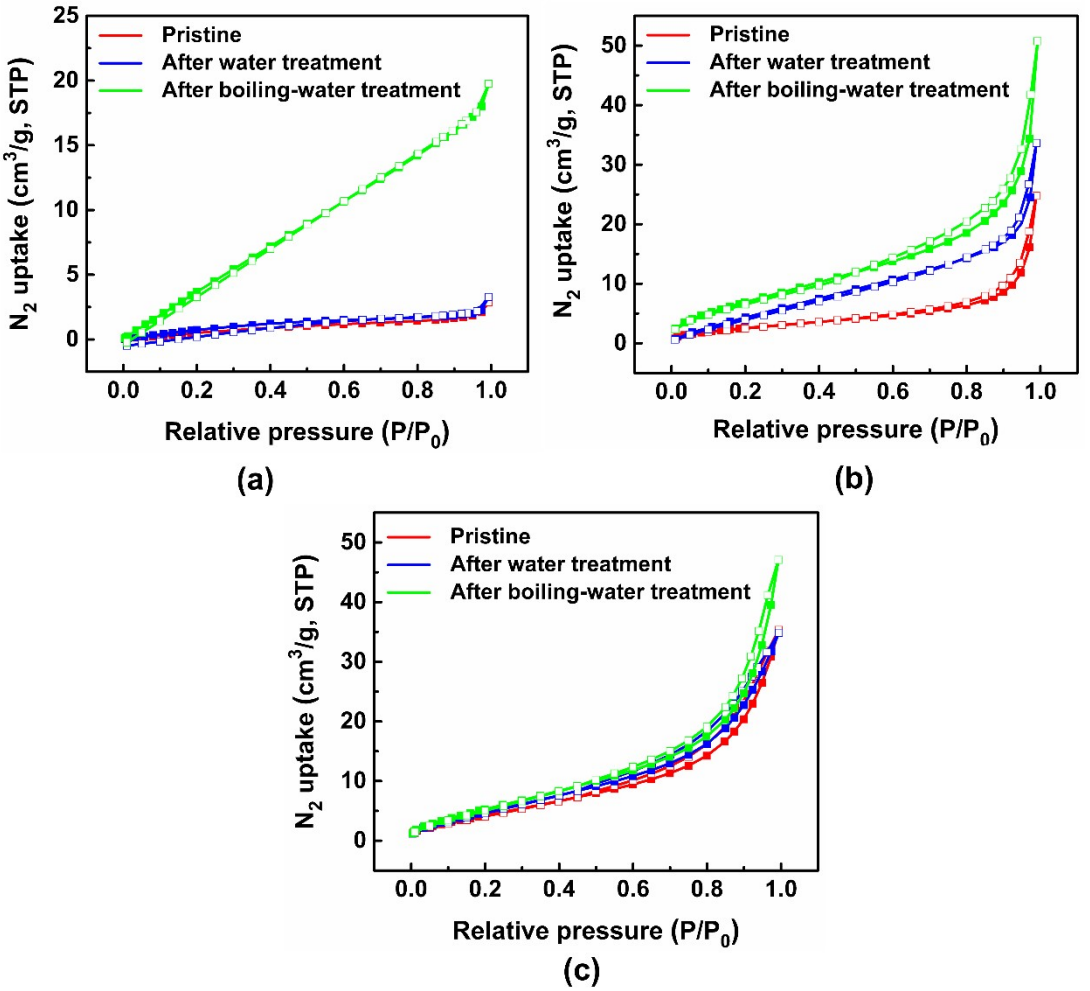

Fig. S6 Nitrogen physisorption isotherms for **Zn-pzdc-H_3O^+** (a), **Mn-pzdc-H_3O^+** (b) and **Cu-Hpzdc-H_2O** (c) at 77 K before and after water treatments.

The porosities of Zn-pzdc-H_3O^+, Mn-pzdc-H_3O^+ and Cu-Hpzdc-H_2O before and after treatments were examined by nitrogen sorption experiments at 77 K. All samples display the type-III gas adsorption behavior (Fig. S7), indicating that there is the weak interaction between adsorbent and adsorbate, i.e., the characteristics of non-porous materials. Furthermore, the pristine Zn-pzdc-H_3O^+ and Zn-pzdc-H_3O^+ samples treated with water and boiling water show the very small BET surface areas of 3.53, 4.68 and 30.63 m^2/g, respectively, (Langmuir surface areas of 2.01, 2.72 and 31.70 m^2/g, respectively), which illustrate that the adsorption properties may come from surface of the bulk materials but not the porosity. Like all Zn-pzdc-H_3O^+ samples, all Mn-pzdc-H_3O^+ and Cu-Hpzdc-H_2O samples show the very similar results (Table S4). After water and boiling-water treatments, Zn-pzdc-H_3O^+, Mn-pzdc-H_3O^+ and Cu-Hpzdc-H_2O

samples exhibit the gradual trends in the surface areas. The results are related to the increase of the size of particles rather than the porous structures of materials, which results from the influence of the external environment and the operating condition, such as water, stirring and heating.

Table S4 BET and Langmuir surface areas of all samples before and after water treatments

Sample	Type of surface area	Pristine	After water treatment	After boiling water treatment
Zn-pzdc-H_3O^+	BET (m^2/g)	3.53	4.68	30.63
	Langmuir (m^2/g)	2.01	2.72	31.70
Mn-pzdc-H_3O^+	BET (m^2/g)	10.41	25.07	29.72
	Langmuir (m^2/g)	10.40	19.26	26.67
Cu-Hpzdc-H_2O	BET (m^2/g)	19.39	22.56	24.88
	Langmuir (m^2/g)	15.01	16.01	17.75

VIII. Stability: IR spectra

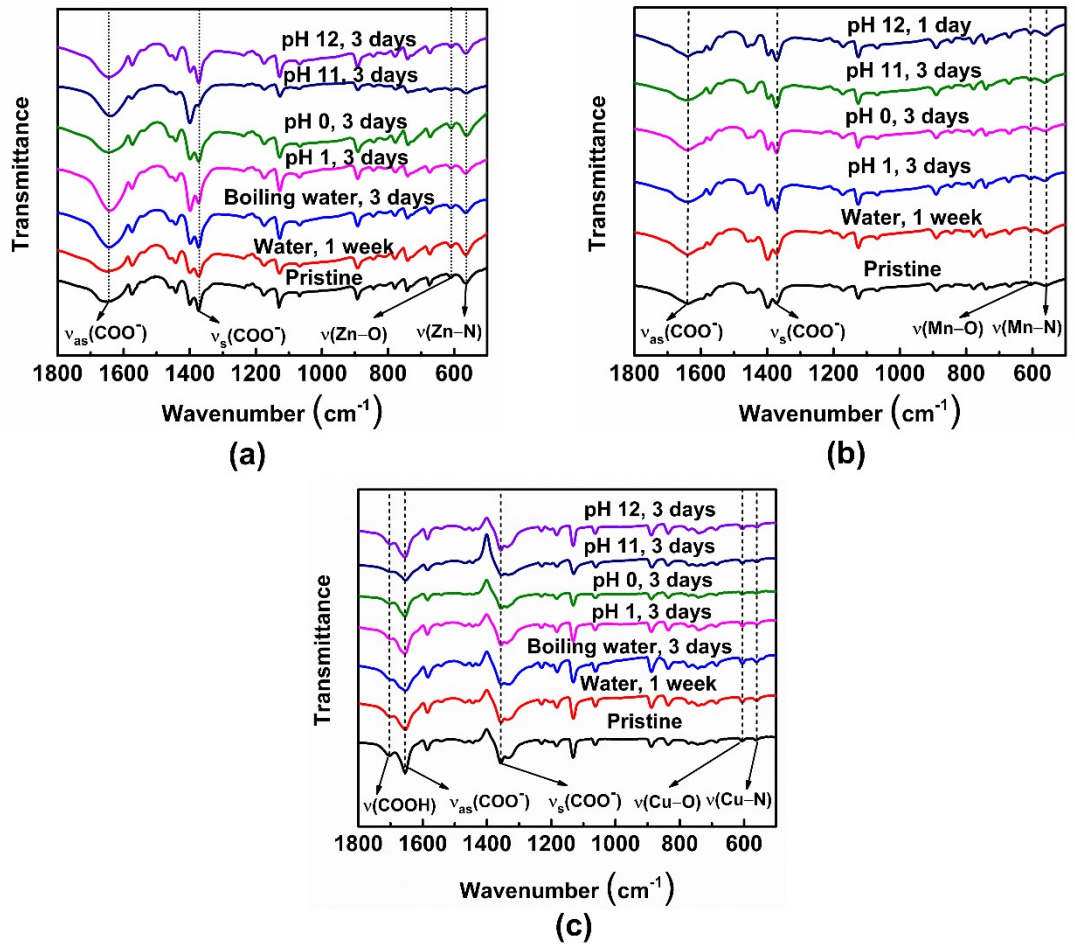

Fig. S7 IR spectra for **Zn-pzdc-H_3O^+** (a), **Mn-pzdc-H_3O^+** (b) and **Cu-Hpzdc-H_2O** (c) before and after treatments (performed on a Nicolet 5700 FT-IR spectrometer).

IX. Stability: PXRD pattern and IR spectrum of Mn-pzdc-H_3O^+ after being treated with boiling water

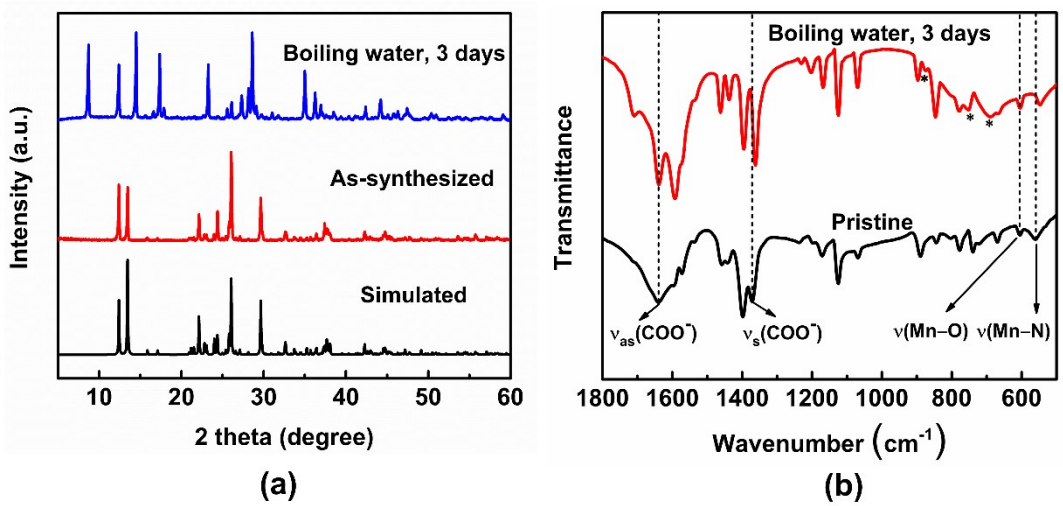

Fig. S8 PXRD pattern (a) and IR spectrum (b) for **Mn-pzdc-H_3O^+** upon immersion of boiling water for 3 days.

After being treated with boiling water for 3 days, Mn-pzdc-H_3O^+ shows some peaks identical to the pristine one and some new unidentified peaks in the PXRD pattern. The above result demonstrates that Mn-pzdc-H_3O^+ partially maintains its structural integrity and partially undergoes phase transitions to form new crystalline structures rather other structural collapse. In the IR spectrum, boiling-water-treated Mn-pzdc-H_3O^+ exhibits most unaltered peaks (such as 1639 cm^{-1} for $\nu_{as}(COO^-)$ and 605 cm^{-1} for ν (Mn–O)), a few changed peaks (just a shift of peak position, 1362 cm^{-1} for $\nu_s(COO^-)$ and 548 cm^{-1} for ν (Mn–N)) , and a few new peaks (denoted as *, 874, 752 and 689 cm^{-1}). These unchanged and changed peaks indicates that there exist coordination bonds in boiling-water-treated sample and the bond lengths are changed only. Some new peaks are possibly associated with the change of coordination bond length, which leads to different vibrations in aromatic ring. Meanwhile, the change in coordination bond length is likely to be related to the generation of new crystalline phases. It is perhaps that the new crystalline phases correspond to more-stable states compared to the pristine Mn-pzdc-H_3O^+ sample.[4]

X. Water adsorption–desorption isotherms

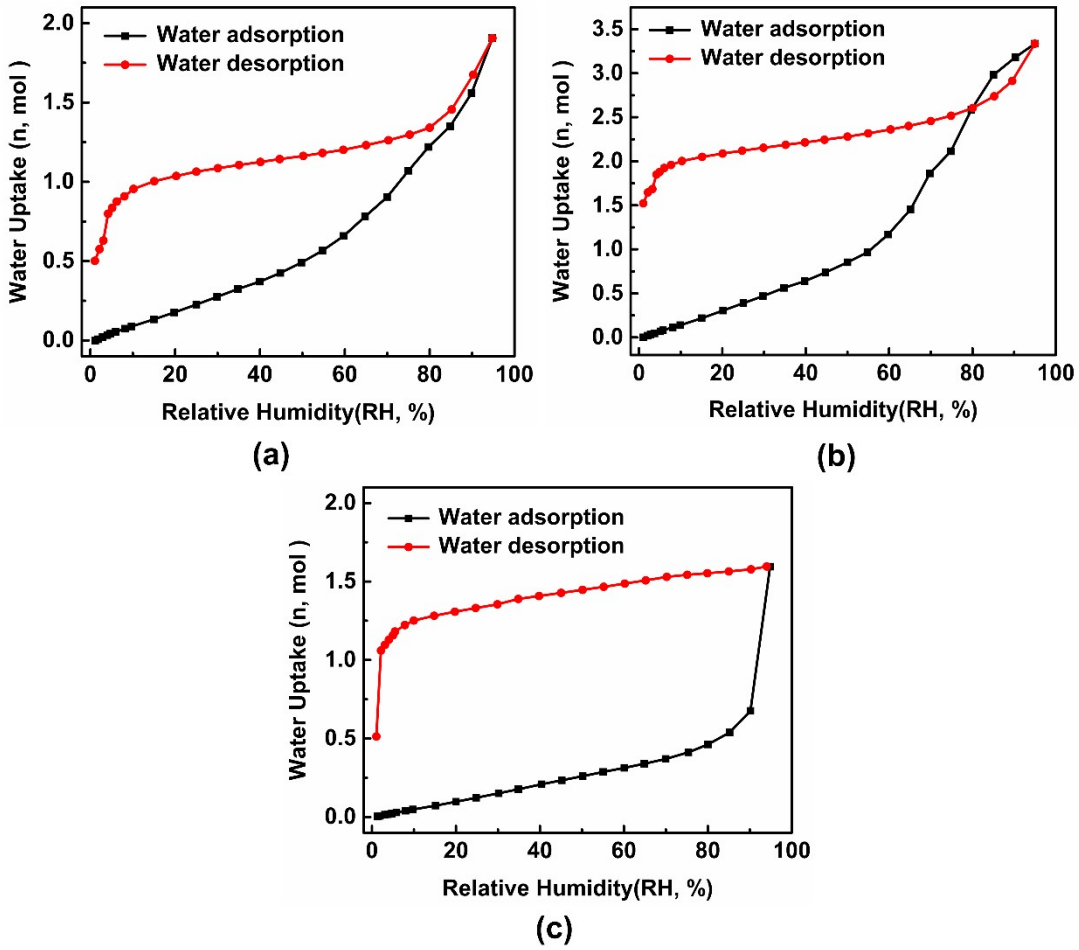

Fig. S9 Water adsorption–desorption isotherms of **Zn-pzdc-H_3O^+** (a), **Mn-pzdc-H_3O^+** (b) and **Cu-Hpzdc-H_2O** (c) at 298 K.

XI. Electrochemical measurements: impedance spectra

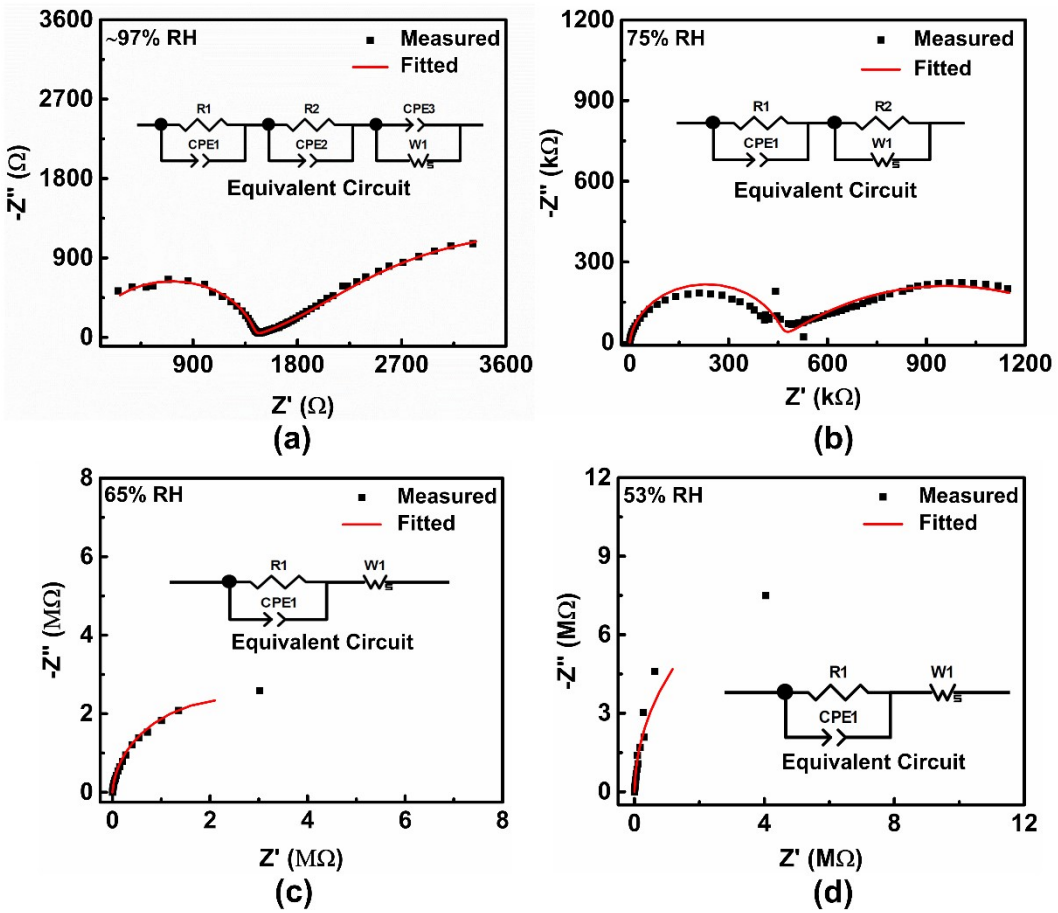

Fig. S10 Nyquist plots of **Zn-pzdc-H_3O^+** at different RH (relative humidity) and 298 K (R1, bulk resistor; R2, grain boundary resistor; CPE, constant phase element; W1, Warburg diffusion element).

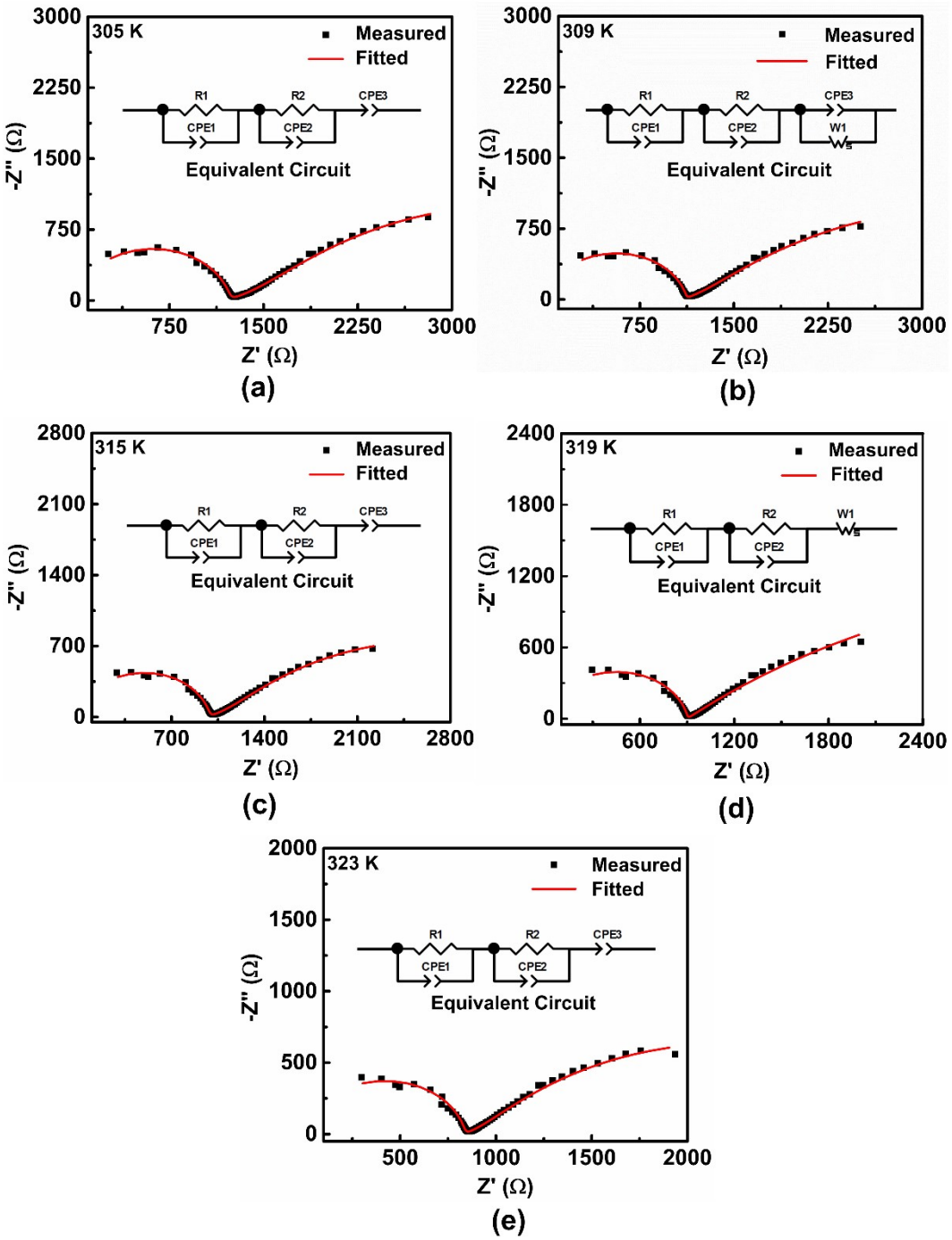

Fig. S11 Nyquist plots of **Zn-pzdc-H_3O^+** at different temperatures and ~97% RH (relative humidity) (R1, bulk resistor; R2, grain boundary resistor; CPE, constant phase element; W1, Warburg diffusion element).

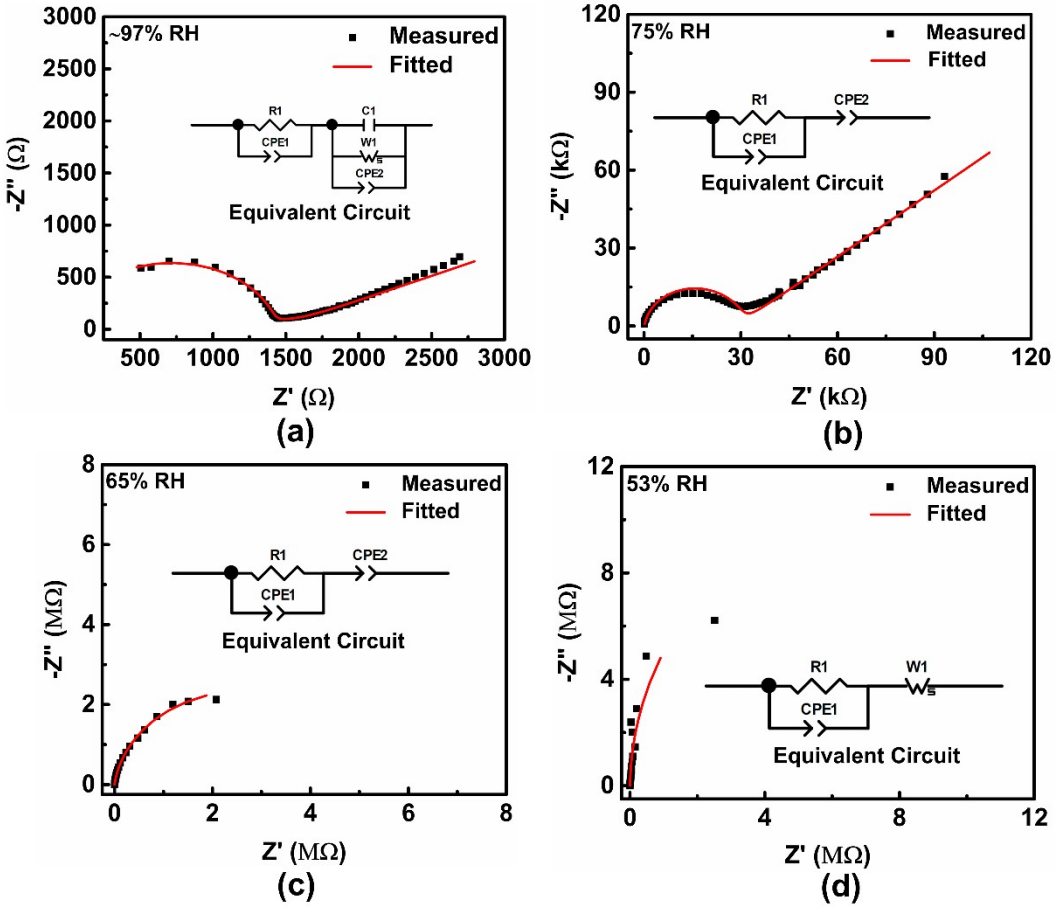

Fig. S12 Nyquist plots of **Mn-pzdc-H_3O^+** at different RH (relative humidity) and 298 K (R1, bulk resistor; CPE, constant phase element; C1, capacitor; W1, Warburg diffusion element).

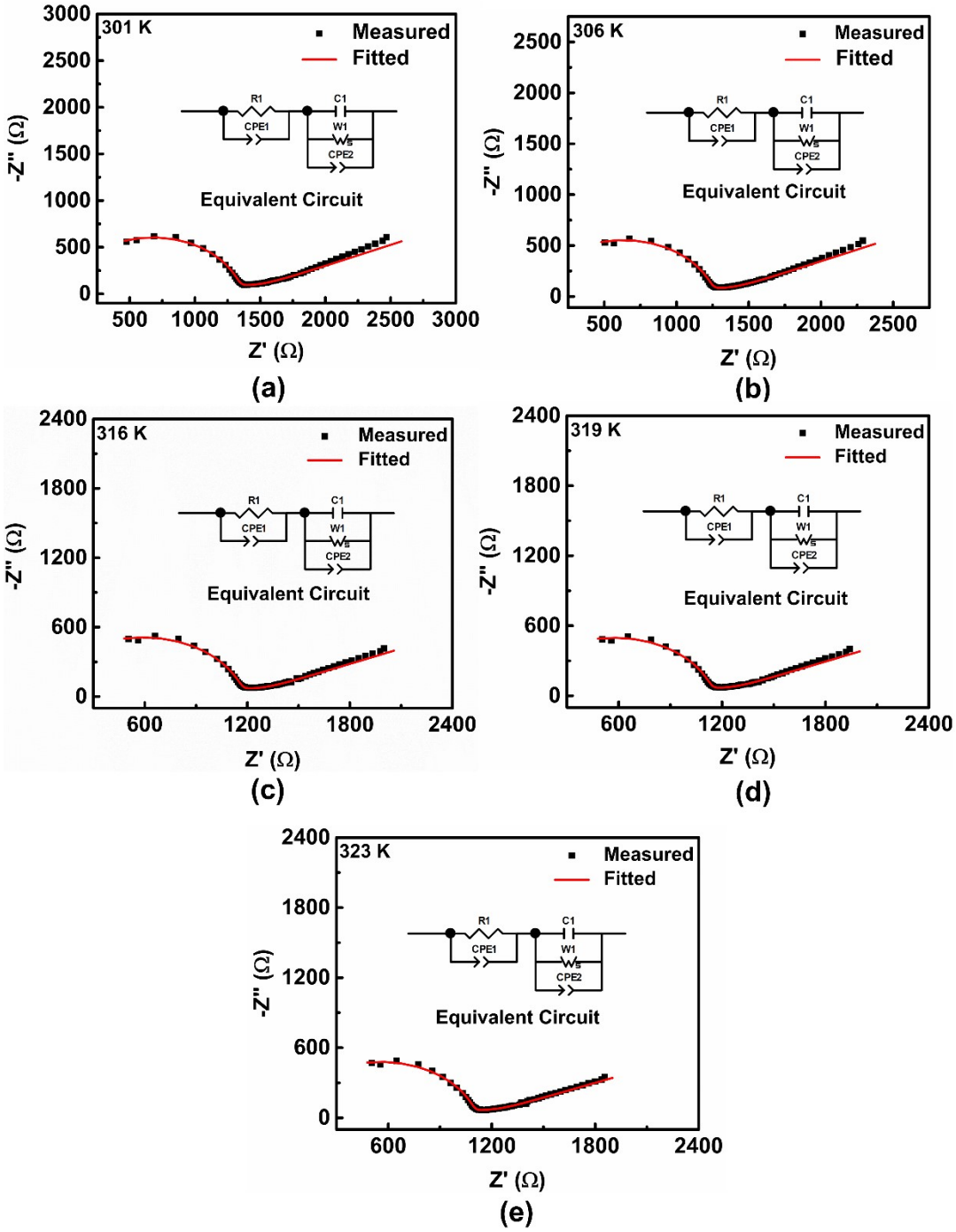

Fig. S13 Nyquist plots of **Mn-pzdc-H_3O^+** at different temperatures and ~97% RH (relative humidity) (R1, bulk resistor; CPE, constant phase element; C1, capacitor; W1, Warburg diffusion element).

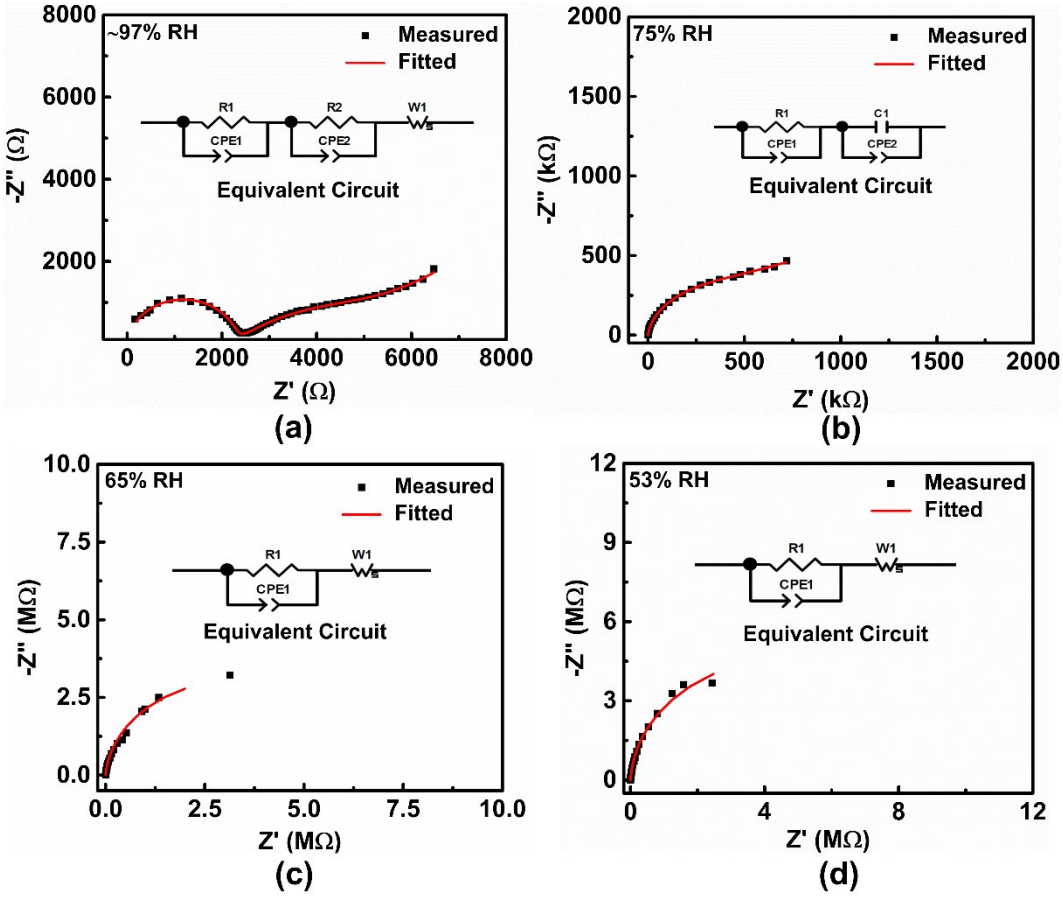

Fig. S14 Nyquist plots of **Cu-Hpzdc-H_2O** at different RH (relative humidity) and 298 K (R1, bulk resistor; R2, grain boundary resistor; CPE, constant phase element; C1, capacitor; W1, Warburg diffusion element).

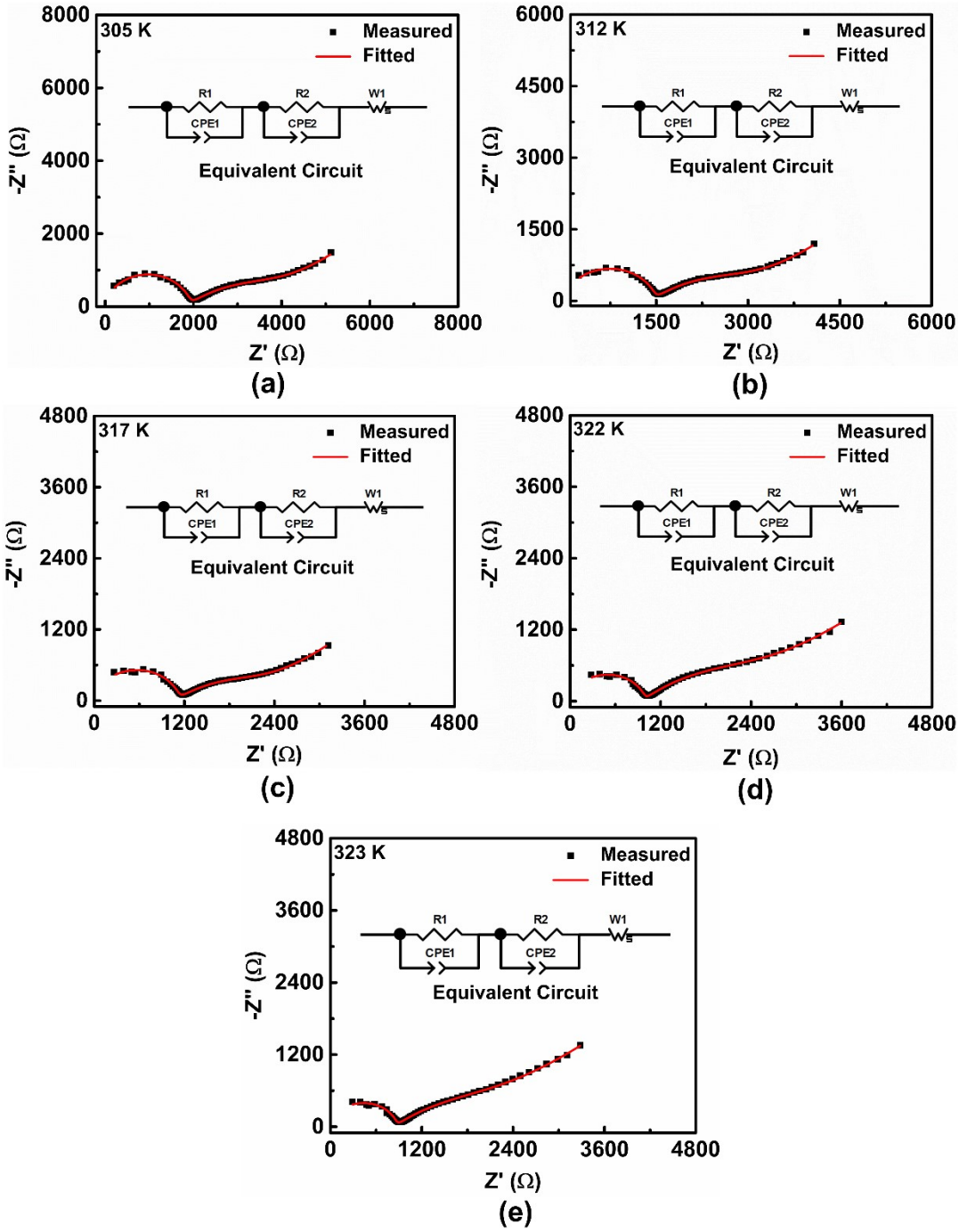

Fig. S15 Nyquist plots of **Cu-Hpzdc-H_2O** at different temperatures and ~97% RH (relative humidity) (R1, bulk resistor; R2, grain boundary resistor; CPE, constant phase element; W1, Warburg diffusion element).

XII. PXRD patterns after impedance measurements.

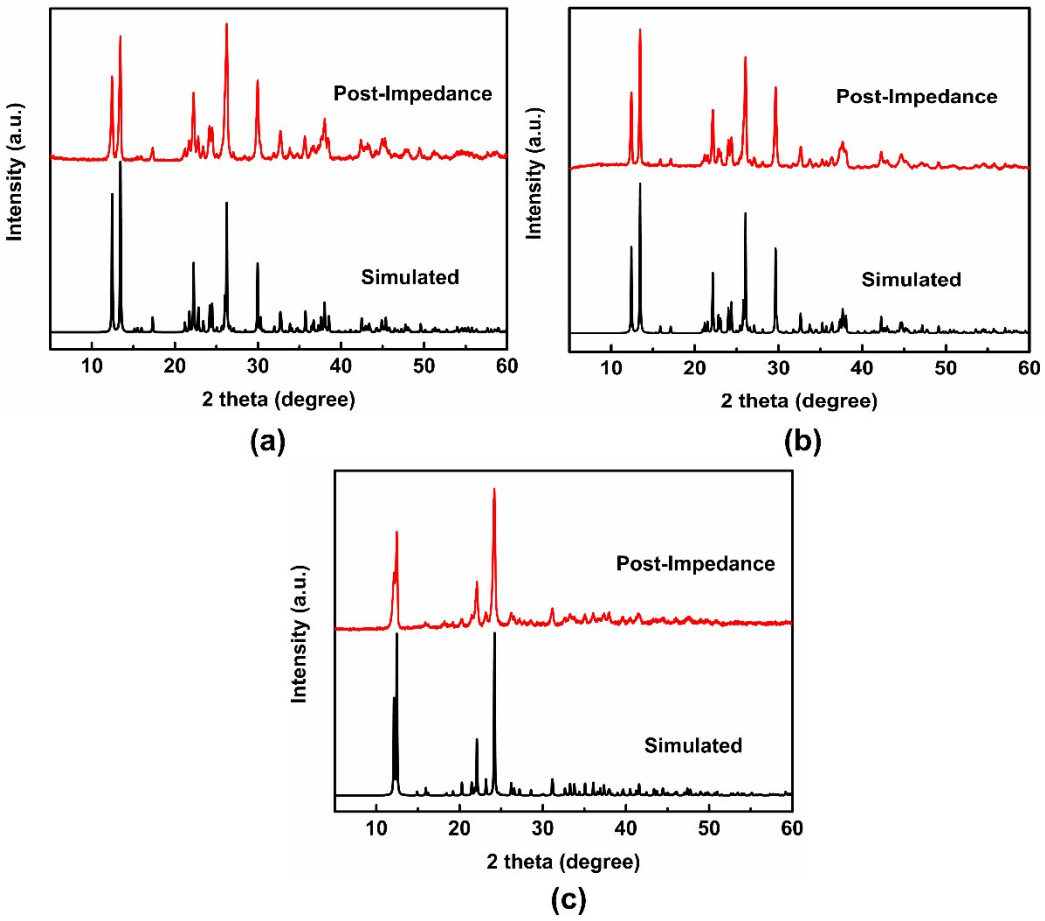

Fig. S16 (a) PXRD patterns of simulations based on single-crystal analysis and after the impedance measurements for **Zn-pzdc-H_3O^+** (a), **Mn-pzdc-H_3O^+** (b) and **Cu-Hpzdc-H_2O** (c) (at ~97% RH and 298–323 K).

XIII. Comparison of chemical stability

Table S5 Comparison of chemical stability of Zn-pzdc-H_3O^+, Mn-pzdc-H_3O^+ and Cu-Hpzdc-H_2O with reported MOF materials.

Materials	pH range	Time (day or hour)	References
Zn-pzdc-H_3O^+	0–12	3 days	This work
Cu-Hpzdc-H_2O	0–12	3 days	This work
Mn-pzdc-H_3O^+	0-11 12	3 days 1 day	This work
MIP-202(Zr) [a]	0–12	–	5
PCN-230	0–12	12 hours	6
PCN-225	0–12	12 hours	7
$[H_2en]_4[Ni_5(OH)_3(trzS)_3(en)(H_2O)(B\text{-}\alpha\text{-}PW_9O_{34})]\cdot 6H_2O$ [b]	2–12	48 hours	8
$[Cu_3(\mu_3\text{-}OH)(H_2O)_3(atz)_3]_3[P_2W_{18}O_{62}]\cdot 14H_2O$ [c]	2–12	20 hours	9
$Cu_6(trz)_{10}(H_2O)_4[H_2SiW_{12}O_{40}]\cdot 8H_2O$ [d]	2–12	24 hours	10
$[Zn_{12}(trz)_{20}][SiW_{12}O_{40}]\cdot 11H_2O$ [e]	2–13	24 hours	11
$\{[Cu^I_3Cu^{II}_3L_3(DMF)_2(CH_3OH)(H_2O)]\cdot 3CH_3OH\}_n$ [f]	1–9	1 day	12
$[Ni_3(HL)_2(H_2O)_{10}]\cdot 4H_2O$ [g]	1.99–6.23	4 days	13
$[Eu_{20}(PDC)_{12}(SO_4)_{12}(\mu_2\text{-}OH)_3(\mu_2\text{-}H_2O)_3(H_2O)_{36}]_n$ [h]	2–13	12 hours	14
$Zn_3(IBT)_2(H_2O)_2$ [i]	2–12	24 hours	15
$\{[Sr(o\text{-}CPhH_2IDC)(H_2O)_2]\cdot 2H_2O\}_n$ [g]	1–11	1 day	16
[FcCO-$(CH_2)_2$COOH] [k]	1–6	24 hours	17
$Ni_3(BTP)_2$ [l]	2-14	14 days	18
UiO-66-NO_2 [m]	1–14	2 hours	19
$[(CH_3)_2NH_2]_2[Eu_6(\mu_3\text{-}OH)_8(1,4\text{-}NDC)_6(H_2O)_6]$ [n]	3.5–10	24 hours	20

[a] Ligand = L-aspartic acid. [b] en = ethylenediamine, H_2trzS = 1H-1,2,4-triazole-3-thiol. [c] Hatz = 3-amino-1,2,4-triazolate. [d] [e] Trz =1,2,4-triazole. [f] H_3L = [3-(4-methyl-benzoyl)-thioureido]-acetic acid. [g] H_4L = 4-F-$C_6H_4CH_2N(CH_2PO_3H_2)_2$. [h] H_3PDC =3,5-pyrazoledicarboxylic acid. [i] 4,5-bis(tetrazol-5-yl)imidazole.[j] o-$CPhH_4IDC$ = 2-(2-carboxylphenyl)-1H-imidazole-4,5-dicarboxylic acid. [k] Fc = (η^5-C_5H_5)Fe(η^5-C_5H_4). [l] H_3BTP = 1,3,5-tris(1*H*-pyrazol-4-yl)benzene. [m] Ligand = 2-nitro-benzenedicarboxylic acid. [n] 1,4-NDC = 1,4-naphthalenedicarboxylate.

XIV. Comparison of proton conductivity

Table S6 Comparison of proton conductivity of Zn-pzdc-H_3O^+, Mn-pzdc-H_3O^+ and Cu-Hpzdc-H_2O with some reported proton conductors.

Materials	Proton Conductivity (S/cm)	Activation Energy (eV)	Temperature (K)	RH (%)	References
Zn-pzdc-H_3O^+	2.42×10^{-3}	0.21			
Mn-pzdc-H_3O^+	2.03×10^{-3}	0.10	323	~97	This Work
Cu-Hpzdc-H_3O	1.68×10^{-3}	0.35			
$[Pb_2(L)(H_2O)]$ [a]	6.61×10^{-4}	0.21	323	98	21
$[Ni_2(H_2L)_2(bpyBr)_2(H_2O)_3]_n$/Nafion [b]	7.43×10^{-7}	0.159	333	–	22
$[Eu_2(HBDPP)_2(H_2O)_2(DMF)_2](H_2O)_2$ [c]	4.53×10^{-4}	0.17 0.42	348	98	23
$[Zn(L)Cl]_n$ [d]	1.16×10^{-3}	0.37 0.42	343	98	24
$\{[Co_2(AHP)_5(DMA)_2](1,5\text{-}NDS)_2(DMA)_2(H_2O)_3(S)\}$ [e]	1.93×10^{-3}	0.21	363	98	25
$[Zn(p\text{-}IPhHIDC)]_n$ [f]	1.9×10^{-3}	0.64	373	98	26
$[Co(PPA)_2(BDC)(H_2O)_2\cdot(PPA)_2(H_2BDC)_2(H_2O)]$ [g]	1.20×10^{-4}	0.24	298	~97	27
$(H_2L2)_{0.5}[(Cu^{I}L2)_2(PMo_{12}O_{40})]\cdot H_2O$ [h]	1.9×10^{-4}	0.43	338	95	28
$Mn(C_2O_4)(C_{12}H_{14}N_6O_2)$ [i]	1.1×10^{-4}	0.41	298	98	29
$[Bi_4(HAzoBTC)_2(AzoBTC)(OH)_2(H_2O)_4]\cdot7H_2O$ [j]	1.0×10^{-4}	–	353	80	30
UMOM-100-b [k]	2.11×10^{-4}	0.66	353	90	31
$[Cu_4(S,S \text{ or } R,R\text{-}LOH)_3(NO_3)\cdot3H_2O]_n$ [l]	0.64×10^{-4}	0.34	298	97	32
(R)-$[Ni(pemp)(H_2O)_2]$ [m]	1.61×10^{-4}	0.24	298	95	33
$\{[Cu(H_2L)(H_2O)_2]_2[PW_{12}O_{40}]\}\{[Cu(HL)(H_2O)_2]_2[PW_{12}O_{40}]\}\cdot4CH_3OH\cdot4H_2O$ [n]	1.05×10^{-4}	0.16	298	98	34
$\{Cd_2(D\text{-}pmpcH)(H_2O)_2Cl_2\}_n$ [o]	1.38×10^{-4}	0.14	323	~97	35
Mg-BPTC [p]	2.60×10^{-4}	0.47, 1.18	373	98	36
$\{[Co_3(p\text{-}ClPhHIDC)_3$	2.47×10^{-4}	0.20	363	93	37

$(H_2O)_3]\cdot 6H_2O\}_n$ [q]					
Co(*m*-BrPhIDC)$_2$ $(H_2O)_6]\cdot 2H_2O$ [r]	0.76×10^{-4}	0.56	373	98	38
$\{[Eu_3(bpydb)_3(HCOO)(OH)_2(DMF)]\cdot 3DMF\cdot xH_2O\}_n$ [s]	1.7×10^{-4}	0.63	325	98	39
$\{[Er_3(pmpc)(C_2O_4)_3(H_2O)_7]\cdot 2H_2O\}_n$ [t]	0.81×10^{-4}	0.33	298	~97	40
PA@Tp-Stb [u]	2.3×10^{-5}	–	332	98	41
$(H_{12}RCC1)^{12+}\cdot 6(SO_4)^{2-}\cdot 27.25(H_2O)$ [v]	0.61×10^{-4}	0.10	303	95	42
$CB[8]\cdot 6.8HCO_2H\cdot 13H_2O$ [w]	1.3×10^{-4}	0.56	298	98	43
$[(H_3betc)(H\text{-}Hopip)_{0.5}\cdot(H_2O)]$ [x]	1.34×10^{-4}	0.41	298	~97	44
GINZH [y]	1.1×10^{-4}	0.20	307	98	45
GISH [z]	2.0×10^{-4}	0.39	293	98	46

[a] H_4L = biphenyl-3,3′,5,5′-tetracarboxylic acid . [b] H_4L = 5,5'-(butane-1,4-diylbis(oxy)) diisophthalic acid, and bpyBr = 4,4'-dibromo-2,2′-bipyridyl. [c] H_4BDPP = 3,5-bis(3,5-dicarboxylphenyl)pyridine, and DMF = *N*,*N*-dimethylformamide. [d] HL = 2-(1-(carboxymethyl)-1H-benzo[d]imidazol-3-ium-3-yl)acetate. [e] AHP = 1,1′-(anthracene-9,10-diylbis(methylene))bis-(pyridin-1-ium-4-olate, DMA = Dimethylacetamide and 1,5-NDS = 1,5-naphthalenedisulfonic acid.

[f] p-IPhH_3IDC= *p*-N-imidazol-1-yl-phenyl-1*H*-imidazole-4,5-dicarboxylic acid. [g] PPA = 4-(3-pyridinyl)-2-amino pyrimidine, H_2BDC = 1,4-benzenedicarboxylic acid. [h] L2 = 1, 4-bis((1H-1,2,4-triazol-1-yl)methyl)-benzene. [i] $C_{12}H_{14}N_6O_2$ = cyclic dipeptides generated by racemic histidine molecules. [j] H_4AzoBTC = 3,3′,5,5′-azobenzenetetracarboxylic acid. [k] UMOM-100-b = the incorporation of acid functionalized Cu(II)-based nanosized cuboctahedron MOP into a mesoporous MOF, PCN-777. [l] S,S or R,R-LOH = (S,S or R,R)-3,5-bis-(1-hydroxyethyl)-1,2,4-triazolate). [m] $pemp^{2-}$ = (R)-(1-phenylethylamino)-methylphosphonate. [n] H_2L = 4,4′-bis(hydroxymethyl)-2,2′-bipyridine. [o] D-H_3pmpc = (D)-1-(phosphono-methyl)piperidine-3-carboxylic acid. [p] H_4BPTC = 2,2',6,6'- tetracarboxybiphenyl. [q] *p*-ClPhH_3IDC = 2-(p-chloro-phenyl)-imidazole-4,5-dicarboxylic acid. [r] *o*-BrPhH_3IDC = 2-(o-bromo-phenyl)-imidazole-4,5-dicarboxylic acid. [s] bpydbH_2 = 4,4′-(4,4′-bipyridine-2,6-diyl) dibenzoic acid, DMF = *N*,*N*′-dimethyl -formamide. [t] H_3pmpc = 1-(phosphonomethyl)piperidine-3-carboxylic acid.[u] PA = loaded H_3PO_4, Tp = triformylphloroglucinol, Stb = 4,4′-diaminostilbene. [v] H_{12}RCC1 = a porous organic cage material. [w] CB8 = cucurbit[8]uril. [x] H_4betc = 1,2,4,5-benzenetetracarboxylic acid, Hopip = homopiperazine. [y] GINZH = a gallic acid-isoniazid cocrystal compound. [z] GISH = a hydrated sulfuric salt of gallic acid and isoniazid.

XV. References for Supporting Information

1 M. Gryz, W. Starosta and J. Leciejewicz, *J. Coord. Chem.*, 2005, **58**, 931.

2 (a) J. Zou, Y. Wu, X. Wei, C. Duan, Y. Liu and Z. Xu, *Transition Met. Chem.*, 1998, **23**, 481; (b) L. Mao, S. J. Rettig, R. C. Thompson, J. Trotter and S. Xia, *Can. J. Chem.*, 1996, **74**, 433.

3 (a) F. Nepveu and M. H. Berkaoui, *Acta Cryst.*, 1993, **C49**, 1465; (b) L. Mao, S. J. Rettig, R. C. Thompson, J. Trotter and S. Xia, *Can. J. Chem.*, 1996, **74**, 2413.

4 A. Schneemann, V. Bon, I. Schwedler, I. Senkovska, S. Kaskel and R. A. Fischer, *Chem. Soc. Rev.*, 2014, **43**, 6062–6096.

5 S. Wang, M. Wahiduzzaman, L. Davis, A. Tissot1, W. Shepard, J. Marrot, C. Martineau-Corcos, D. Hamdane, G. Maurin, S. D. -Vinot and C. Serre, *Nat. Commun.*, 2018, **9**, 4937.

6 T.-F. Liu, D. Feng, Y.-P. Chen, L. Zou, M. Bosch, S. Yuan, Z. Wei, S. Fordham, K. Wang and H.-C. Zhou, *J. Am. Chem. Soc.*, 2015, **137**, 413.

7 H.-L. Jiang, D. Feng, K. Wang, Z.-Y. Gu, Z. Wei, Y.-P. Chen and H.-C. Zhou, *J. Am. Chem. Soc.*, 2013, **135**, 13934.

8 G. J. Cao, J. D. Liu, T. T. Zhuang, X. H. Cai and S. T. Zheng, *Chem. Commun.*, 2015, **51**, 2048.

9 Y. Q. Jiao, H. Y. Zang, X. L. Wang, E. L. Zhou, B. Q. Song, C. G. Wang, K. Z. Shao and Z. M. Su, *Chem. Commun.*, 2015, **51**, 11313.

10 E. L. Zhou, C. Qin, P. Huang, X. L. Wang, W.C. Chen, K. Z. Shao and Z. M. Su, *Chem. Eur. J.*, 2015, **21**, 11894.

11 E. L. Zhou, C. Qin, X. L. Wang, K. Z. Shao and Z. M. Su, *Chem. Eur. J.*, 2015, **21**, 13058.

12 Z. B. Sun, Y. L. Li, Z. H. Zhang, Z. F. Li, B. Xiao and G. Li, *New J. Chem.*, 2019, **43**, 10637.

13 H. Xu, L. Feng, W. Huang, Q. Wang and H. Zhou, *New J. Chem.*, 2019, **43**, 807.

14 L. He, J. Kumar Nath, E. X. Chen, H.-D. Lai, S.-L. Huang and Q. Lin, *Chem. Commun.,* 2019, **55**, 2497.

15 C. Liu, N. Zhao, X. Zou and G. Zhu, *CrystEngComm*, 2018, **20**, 3158.

16 J. Feng, S. Yu, K. Guo, J. Li and G. Li, *Polyhedron*, 2019, **169**, 1.

17 Y. Qin, T. -L. Gao, W. -P. Xie, Z. Li, and G. Li, *ACS Appl. Mater. Interfaces*, 2019, **11**, 31018.

18 V. Colombo, S. Galli, H. J. Choi, G. D. Han, A. Maspero, G. Palmisano, N. Masciocchi and J. R. Long, *Chem. Sci.*, 2011, **2**, 1311.

19 M. Kandiah, M. H. Nilsen, S. Usseglio, S. Jakobsen, U. Olsbye, M. Tilset, C. Larabi, E. A. Quadrelli, F. Bonino and K. P. Lillerud, *Chem. Mater.*, 2010, **22**, 6632.

20 D.-X. Xue, Y. Belmabkhout, O. Shekhah, H. Jiang, K. Adil, A. J. Cairns and M. Eddaoudi, *J. Am. Chem. Soc.*, 2015, **137**, 5034.

21 X. Chen, Z. Zhang, J. Chen, S. Sapchenko, X. Han, I. da-Silva, M. Li, I. J. Vitorica-Yrezabal, G. Whitehead, C. C. Tang, K. Awaga, S. Yang and M. Schröder, *Chem. Commun.*, 2021, **57**, 65.

22 R. Li, H. Liu, C. Zhou, Z. Chu, J. Lu, S. Wang, W. Yan and J. Jin, *Inorg. Chem. Front.*, 2020, **7**, 1880.
23 S. -Fang Zhou, B. -B. Hao, T. Lin, C.-X. Zhang and Q.-L. Wang, *Dalton Trans.*, 2020, **49**, 14490.
24 Z.-Q. Shi, N.-N. Ji, M.-H. Wan, and G. Li, *Inorg. Chem.* 2020, **59**, 4781.
25 A. Mohanty, U. P. Singh, A. Ghorai, S. Banerjee and R. J. Butcher, *CrystEngComm*, 2021, **23**, 684.
26 Y. Qin, M. -H. Xue, B. -H. Dou, Z.-B. Sun and G. Li, *New J. Chem.*, 2020, **44**, 2741.
27 X. Liang, T. Cao, L. Wang, C. Zheng, Y. Zhao, F. Zhang, C. Wen, L. Feng and C. Wan, *CrystEngComm*, 2020, **22**, 1414.
28 K. Lu, A. L. Peláez, L. Wu, Y. Cao, C. Zhu, and H. Fu, *Inorg. Chem.*, 2019, **58**, 1794.
29 J. Shi, J. Li, H. Zeng, G. Zou, Q. Zhang and Z. Lin, *Dalton Trans.*, 2018, **47**, 15288.
30 S. M. F. Vilela, T. Devic, A. Várez, F. Salles and P. Horcajada, *Dalton Trans.*, 2019, **48**, 11181.
31 J. Lee, D. -W. Lim, S. Dekura, H. Kitagawa and W. Choe, *ACS Appl. Mater. Interfaces*, 2019, **11**, 12639.
32 B. Q. Song, D. Q. Chen, Z. Ji, J. Tang, X. L. Wang, H. Y. Zang and Z. M. Su, *Chem. Commun.*, 2017, **53**, 1892.
33 X. -G. Liu, S. -S. Bao, J. Huang, K. Otsubo, J. S. Feng, M. Ren, F. C. Hu, Z. Sun, L. M. Zheng, S. Wei and H. Kitagawa, *Chem. Commun.*, 2015, **51**, 15141.
34 H. Yang, X. Y. Duan, J. J. Lai, Y. Zhao, X. J. Wang and M. L. Wei, *Inorg. Chem.*, 2019, **58**, 446.
35 X. Liang, K. Cai, F. Zhang, J. Liu and G. Zhu, *CrystEngComm*, 2017, **19**, 6325.
36 X. Y. Dong, X. P. Hu, H. C. Yao, S. Q. Zang, H. W. Hou and T. C. W. Mak, *Inorg. Chem.*, 2014, **53**, 12050.
37 X. Liang, B. Li, M. H. Wang, J. Wang, R. L. Liu and G. Li, *ACS Appl. Mater. Interfaces.*, 2017, **9**, 25082.
38 R. L. Liu, L. L. Zhao, W. Dai, C. L. Yang and G. Li, *Inorg. Chem.*, 2018, **57**, 1474.
39 S. L. Yang, P. P. Sun, Y. Y. Yuan, C. X. Zhang and Q. L. Wang, *CrystEngComm*, 2018, **20**, 3066.
40 X. Liang, K. Cai, F. Zhang, J. Liu and G. Zhu, *J. Mater. Chem. A*, 2017, **5**, 25350.
41 S. Chandra, T. Kundu, S. Kandambeth, R. BabaRao, Y. Marathe, S. M. Kunjir, and R. Banerjee, *J. Am. Chem. Soc.,* 2014, **136**, 6570.
42 M. Liu, L. Chen, S. Lewis, S. Y. Chong, M. A. Little, T. Hasell, I. M. Aldous, C. M. Brown, M. W. Smith, C. A. Morrison, L. J. Hardwick and A. I. Cooper, *Nat. Comm.* 2016, **7**, 12750.
43 M. Yoon, K. Suh, H. Kim, Y. Kim, N. Selvapalam and K. Kim, *Angew. Chem., Int. Ed.*, 2011, **50**, 7870.
44 X. Liang, Y. Chen, L. Wang, F. Zhang, Z. Fan, T. Cao, Y. Cao, H. Zhu, X. He, B. Deng, Y. You, Y. Dong and Y. Zhao, *New J. Chem.*, 2019, **43**, 11099.
45 R. Kaur, B. Ponraj, D. Swain, K. B. R. Varma and T. N. G. Row, *Cryst. Growth Des.,* 2015, **15**, 4171.

46 R. Kaur, D. Swain, D. Dutta, K. Brajesh, P. Singh, A. J. Bhattacharyya, R. Ranjan, C. Narayana, J. Hulliger and T. N. G. Row, *J. Phys. Chem. C*, 2017, **121**, 18317.